

Enhancement of valley selective excitation by a linearly polarized two-color laser pulse

Arqum Hashmi,¹ Shunsuke Yamada,¹ Kazuhiro Yabana,^{1,2} and Tomohito Otobe^{1,*}

¹*Kansai Photon Science Institute, National Institutes for Quantum Science and Technology (QST), Kyoto 619-0215, Japan*

²*Center for Computational Sciences, University of Tsukuba, Tsukuba 305-8577, Japan*

(Dated: March 28, 2023)

Here we proposed the valley selective excitations via a two-color ($\omega + 2\omega$) laser field, made by superimposing two linearly polarized pulses at frequencies ω and 2ω . We have studied the intensity ratio between a few-cycle pulse of ω and 2ω laser, and its enhancement factor by employing the time-dependent first-principle calculations. The valley polarization depends on the carrier envelope phases (CEPs) of pulses and the intensity ratio $I_\omega/I_{2\omega}$. We found that the two-color field enhances the valley polarization as much as 1.2 times larger than the single-color pulse. The maximum valley asymmetry is achieved for the intensity ratio $I_\omega/I_{2\omega}$ of 36 with the relative CEP of π . In our previous work, we found that the asymmetric vector potential induces the valley polarization (Phys. Rev. B 105,115403 (2022)). In this work, we find that the asymmetry of the electric field modulates the valley polarization. Our two-color scheme offers a new path toward the optical control of valley pseudospins.

I. INTRODUCTION

Electrons in two-dimensional (2D) hexagonal lattices have an extra degree of freedom in addition to charge and spin named valley pseudospin [1, 2]. Valleys are local minima in the band structure corresponding to different crystal momenta that are located at the K/K' points of the Brillouin zone (BZ) [3, 4]. In the field of valleytronics, 2D layer materials such as graphene [5, 6] and transitional metal dichalcogenides (TMDs) [7–9] are receiving extensive research efforts. Graphene presents the remarkable feature of Dirac fermions [10, 11]. However, the honeycomb structure with equivalent A and B sublattice enforces zero Berry curvature which makes it not an ideal candidate for valley contrasting properties [12]. As opposed to graphene, TMDs monolayers are of particular interest for practical valleytronics applications because of their broken inversion symmetry and strong spin-orbit coupling (SOC).

Lifting the valley degeneracy to create valley polarization has become a central theme in valleytronics [13, 14]. Several methods have been proposed to achieve transient valley polarization such as applying a magnetic field [15], optical Stark effect [16], and proximity effects generated by magnetic substrates [17]. Due to the several practical limitations of the magnetic field, the optical excitations remain a popular way where selective excitation at K or K' can be achieved using a weak circularly polarized field resonant with the bandgap of the material [8, 18, 19]. Depending on its helicity, the field couples to either K/K' valleys.

The valley-dependent optical selection rules suggest that linearly polarized light couples equal to both valleys. It is widely accepted that valley polarization with linearly polarized fields is impossible [4, 20]. In contrast, it is expected that a few-cycle single-color pulse with the

controlled carrier-envelope phase (CEP) can break this situation [21, 22]. Moreover, ultrashort laser pulses offer ultrafast control of electron dynamics [23, 24]. The possibility of generating the valley polarization with linearly polarized pulses offers an alternative route to valleytronics in graphene and TMDs materials [21, 25]. The advantage of linearly polarized pulses is to avoid reliance on resonant pump-probe spectroscopy that is used in TMDs monolayers to break the symmetry between the K and K' valleys.

Electron dynamics under a strong laser field can be described by solving the time-dependent Kohn-Sham (TDKS) equation in real-time referred to as time-dependent density functional theory (TDDFT) [26, 27]. TDDFT is not only been used to describe the linear response in the frequency domain [28, 29] but also has been very successful to describe the nonlinear and nonperturbative dynamics of electrons by intense ultrashort laser pulses [30–32]. The most powerful aspect of TDDFT is its capability to describe electron dynamics under intense laser fields without any empirical parameters. In condensed matter, it is well known that SOC modifies the band structure of solids. Strong SOC not only modifies the band curvature but also changes the bandgap of the material by lifting the spin degeneracy which ultimately can affect the excitation of carriers. Hence the inclusion of the SOC in TDDFT is essential not only to describe the excitation dynamic under a strong laser field but also important to accurately describe the phenomenon such as spintronics [33] or valleytronics [14].

In our previous study, we found that the asymmetric laser field with mono-cycle laser pulse enables the valley polarization by the real-time TDDFT approach with SOC [22]. A two-color laser can also control the asymmetric excitation [34–37]. In this work, we study the enhancement of valley polarization in WSe₂ monolayer via a two-color field. It is possible to create an asymmetric laser field by mixing a fundamental with frequency ω and its second harmonic 2ω . The two pulses intensity ratio and the relative CEP control the valley polarization.

* otobe.tomohito@qst.go.jp

We also compare the valley polarization results of $\omega + 2\omega$ scheme results with the single color (ω) pulse. We found that the valley polarization via two-color-control exceeds the single-color scheme by 1.2 times as the $\omega + 2\omega$ field exhibits more asymmetry in its temporal shape. Our results reveal a convenient new path toward the optical control of valley pseudospins.

II. THEORETICAL FORMALISM

Using the velocity gauge [38], we describe the time evolution of electron orbitals in WSe₂ monolayer under the pulsed electric field by solving the TDKS equation for Bloch orbitals $u_{b,\mathbf{k}}(\mathbf{r}, t)$ (which is a two-component spinor. b is the band index and \mathbf{k} is the 2D crystal momentum of the thin layer) as,

$$i\hbar \frac{\partial}{\partial t} u_{b,\mathbf{k}}(\mathbf{r}, t) = \left[\frac{1}{2m} \left(-i\hbar\nabla + \hbar\mathbf{k} + \frac{e}{c} \mathbf{A}^{(t)}(t) \right)^2 - e\varphi(\mathbf{r}, t) + \hat{v}_{\text{NL}}^{\mathbf{k} + \frac{e}{\hbar c} \mathbf{A}^{(t)}(t)} + v_{\text{xc}}(\mathbf{r}, t) \right] u_{b,\mathbf{k}}(\mathbf{r}, t), \quad (1)$$

where the scalar potential $\varphi(\mathbf{r}, t)$ includes the Hartree potential from the electrons plus the local part of the ionic pseudopotentials and we have defined $\hat{v}_{\text{NL}}^{\mathbf{k}} \equiv e^{-i\mathbf{k}\cdot\mathbf{r}} \hat{v}_{\text{NL}} e^{i\mathbf{k}\cdot\mathbf{r}}$. Here, \hat{v}_{NL} and $v_{\text{xc}}(\mathbf{r}, t)$ are the non-local part of the ionic pseudopotentials and exchange-correlation potential, respectively.

TDKS equation combined with the Maxwell equations can describe the light propagation in thin layers as well. For this purpose, we assume the spatially uniform macroscopic electric field inside the layer (in our case monolayer is in the xy plane and the light pulse propagates along the z axis) [39, 40]. By using the Maxwell equations, the propagation of the macroscopic electromagnetic fields in the form of the vector potential $\mathbf{A}(z, t)$ is described as,

$$\left(\frac{1}{c^2} \frac{\partial^2}{\partial t^2} - \frac{\partial^2}{\partial z^2} \right) \mathbf{A}(z, t) = \frac{4\pi}{c} \mathbf{J}(z, t), \quad (2)$$

where $\mathbf{J}(z, t)$ is the macroscopic current density of the thin layer.

Under the assumption of zero thickness and spatially uniform electric field inside the monolayer, we can approximate the macroscopic electric current density in Eq. (2) as

$$\mathbf{J}(z, t) \approx \delta(z) \mathbf{J}_{2\text{D}}(t), \quad (3)$$

where $\mathbf{J}_{2\text{D}}(t)$ is 2D current density (current per unit area) of the thin layer.

By treating it as a boundary value problem where reflected (transmitted) fields can be determined by the connection conditions at $z = 0$, we can get the $\mathbf{J}_{2\text{D}}(t)$ as follows,

$$\begin{aligned} \mathbf{J}_{2\text{D}}(t) = & -\frac{e}{m} \int dz \int_{\Omega} \frac{dx dy}{\Omega} \sum_{b,\mathbf{k}}^{\text{occ}} u_{b,\mathbf{k}}^{\dagger}(\mathbf{r}, t) \\ & \times \left[-i\hbar\nabla + \hbar\mathbf{k} + \frac{e}{c} \mathbf{A}^{(t)}(t) + \frac{m}{i\hbar} \left[\mathbf{r}, \hat{v}_{\text{NL}}^{\mathbf{k} + \frac{e}{\hbar c} \mathbf{A}^{(t)}(t)} \right] \right] u_{b,\mathbf{k}}(\mathbf{r}, t), \end{aligned} \quad (4)$$

where Ω is the area of the 2D unit cell and the sum is taken over the occupied orbitals in the ground state. The detail of our formalism is explained in the references [22, 39].

The method explained above is implemented in the TDDFT package named Scalable Ab initio Light-Matter simulator for Optics and Nanoscience (SALMON). Full details of the SALMON code and its implementation are described elsewhere [41, 42].

The lattice parameter of WSe₂ monolayer is chosen to be 3.32 Å. The vacuum distance of 20 Å was employed in the direction normal to the interface. The exchange-correlation potential utilizes the adiabatic local-density approximation with Perdew-Zunger functional [43]. We use a spin non-collinear treatment for the exchange-correlation potential [44, 45]. The dynamics of the 12 valence electrons for one W atom, and 12 valence electrons for two Se atoms are treated explicitly while the effects of the core electrons are considered through norm-conserving pseudopotentials [46]. The total energy convergence criterion was set to 10^{-8} eV. For such calculations, the spatial grid sizes and k-points are optimized. The converged results were obtained with a fine r-grid and k-grid of 0.21 Å and $15 \times 15 \times 1$ k-mesh respectively. We use the vector potential for the fundamental laser pulse and its second harmonics pulses with the following waveform,

$$\begin{aligned} A(t) = & -\frac{c}{\omega} f(t) \left[E_{\omega} \cos \left\{ \omega \left(t - \frac{T_P}{2} \right) + \varphi_{\omega} \right\} \right. \\ & \left. + \frac{1}{2} E_{2\omega} \cos \left\{ 2\omega \left(t - \frac{T_P}{2} \right) + \varphi_{2\omega} \right\} \right] \end{aligned} \quad (5)$$

where, E_{ω} and $E_{2\omega}$ are the peak electric field amplitudes while φ_{ω} and $\varphi_{2\omega}$ are CEP of the fundamental pulse and its second harmonics respectively. ω is the carrier frequency and T_P is the total pulse duration. The pulse envelope function is of \cos^4 shape for the vector potential given as

$$f(t) = \begin{cases} \cos^4 \left(\pi \frac{t - T_P/2}{T_P} \right) & 0 \leq t \leq T_P \\ 0 & \text{otherwise} \end{cases}. \quad (6)$$

We use the linearly polarized pulses with 0.4 eV frequency for the fundamental and its second harmonic (0.8 eV). Both pulse lengths are set to $T_P = 10$ fs and the small time step size of 5×10^{-4} fs is used for stable calculations.

III. RESULTS AND DISCUSSION

For the molecules, the asymmetric behavior with the intensity ratio $I_\omega/I_{2\omega}$ around four have been used with the photon energy far below the ionization potential [34, 35]. Here, I_ω and $I_{2\omega}$ are the intensity of ω and 2ω pulses respectively. Since we assume the frequencies comparable to the bandgap of WSe₂, the electronic response is significantly different for ω and 2ω . Therefore, we have to clarify the electron dynamics under each color field before proceeding with the two-color field.

Fig. 1(a) shows the vector potential of both pulses. The field intensity of $I = 10^{10}$ W/cm² is used for ω and 2ω pulses, the laser intensity is chosen to induce the non-linear dynamics but be below the damage threshold for monolayer TMDs [47, 48]. In our previous study, we have shown that the polarization parallel to Γ - K experiences different band curvature and hence induces a high degree of valley polarization that can be controlled by CEP [22]. Thus the direction of the polarization of the incident light is considered along the Γ - K . Fig. 1(b) displays the excitation dynamics regarding excitation energy and excited electrons. In the case of ω -field, the excitation energy and the excited electrons are noticeable during the pulse irradiation, and the electronic state returns to its ground state when the pulse ends. The energy per electron is about 8-photon (3.16 eV/electron), which is higher than the expected lowest excitation path (4-photon). On the other hand, in the case of 2ω field, more electrons are excited as compared to ω and the excited electrons remain finite after the pulse ends. The absorbed energy per electron is about 1.52 eV/electron, which indicates the lowest order of the photo-absorption, the two-photon absorption, is dominant. The Keldysh parameter is around 2 for ω -field and 4 for 2ω -field. These results suggest that the excitation process under ω -field is highly non-linear than 2ω , and is in the intermediate stage between multi-photon and tunneling processes.

Fig. 1(c) shows the comparison of the valley polarization by ω and 2ω fields. The valley polarization is defined as,

$$\text{Polarization} = \frac{\rho_{K'} - \rho_K}{\frac{1}{2}(\rho_{K'} + \rho_K)}, \quad (7)$$

where $\rho_K(\rho_{K'})$ are electron densities, obtained by integrating the conduction band electron population around $K(K')$ point. Strong valley polarization is observed by ω -pulse while the 2ω -field does not show any significant valley polarization. The photo-current indicates the sensitivity of the system for each frequency, shown in Fig. 1(d). The current ratio for 2ω is roughly twice of ω -pulse. The large difference in the photo-current between 2ω and ω -pulses indicates that we have to find a good ratio $I_\omega/I_{2\omega}$ to enhance the asymmetric valley polarization.

According to our previous work[22], the valley polarization with the mono-cycle pulse shows the peak with

the phase of $\varphi = \pi/2$ and $3\pi/2$. Regarding the relative phase (φ_{rel}), the intense asymmetric response of molecules has been reported with the 0 and π [49]. Fig. 2(a) shows the valley polarization by changing the E_ω field while the $E_{2\omega}$ is fixed at 10^{10} W/cm², that is intense 2ω pulse case. The CEPs are set as $\varphi_\omega = \pi/2$ and $\varphi_{2\omega} = 3\pi/2$ to induce the best valley polarization. Intense 2ω results in two-photon absorption which leads the K and K' valleys equally excited. Hence no valley asymmetry is present in this case.

Fig. 2(b) shows the valley polarization by changing the $E_{2\omega}$ with intense E_ω . The valley polarization increases as the $E_{2\omega}$ decreases which distinctly indicates the change in the excitation process from the two-photon absorption to tunneling. Fig. 2 confirms that the maximum valley polarization is observed for the $E_\omega/E_{2\omega}$ ratio of 6. The ratio of field $E_\omega/E_{2\omega} = 6$ corresponds to the intensity ratio of $I_\omega/I_{2\omega} = 36$. It should be noted that the ratio $I_\omega/I_{2\omega} = 4$, which is the ratio used in the molecule case, does not work (Fig. 2(b)). For further calculations, we have fixed the laser intensity of the fundamental pulse to $I_\omega = 1 \times 10^{10}$ W/cm² while the superimposed $\omega + 2\omega$ optimized ratio $I_\omega/I_{2\omega}$ is fixed to 36.

Next, we investigate the distribution of excited state electrons in the reciprocal space. The excited electron population is defined as,

$$\rho_{\mathbf{k}}(t) = \sum_{c,v} \left| \int_{\Omega} d^3r u_{v,\mathbf{k}}^*(\mathbf{r}, t) u_{c,\mathbf{k}+\frac{e}{\hbar c}\mathbf{A}(t)}^{\text{GS}}(\mathbf{r}) \right|^2, \quad (8)$$

where v and c are the indices for the valence and conduction bands, respectively, and $u_{b,\mathbf{k}}^{\text{GS}}(\mathbf{r}) = u_{b,\mathbf{k}}(\mathbf{r}, t = 0)$ is the Bloch orbital in the ground state.

Fig. 3(b) shows the maximum population asymmetry at K and K' valley corresponds to vector potential shown in Fig. 3(a). One can see that positive vector potential favors the K' valley. As the φ_ω changes from $3\pi/2$ to $\pi/2$ the waveform of the vector potential changes from positive to negative as shown in Fig. 3(c). Reversing the φ of ω -pulse ($-\pi/2$ ($3\pi/2$) \rightarrow $\pi/2$) switch the valley asymmetry from K' to K valley as shown in Fig. 3(d) suggests a robust mechanism for valley selection.

Fig. 4(a) shows the valley polarization as a function of the $\varphi_{2\omega}$ at numerous CEP of φ_ω . As described above, no asymmetry is observed at $\varphi_\omega = 0$. Consequently, the valley polarization is zero regardless of the $\varphi_{2\omega}$. The valley polarization increases as we change the φ_ω . The valley polarization has the order of $\varphi_\omega = 3\pi/2 > \varphi_\omega = 1.625\pi > \varphi_\omega = 7\pi/4$ and the maximum value is as high as 26%. Valley polarization via two-color-control exceeds the single-color scheme by 1.2 times as the $\omega + 2\omega$ field exhibits more asymmetry in its temporal shape. An increase in the valley polarization as compared to the single-color value indicates that the addition of the 2ω field significantly affects the valley polarization. The phase dependence of the valley polarization shows that the φ_{rel} between ω and 2ω is crucial to tune the valley polarization. It is also worth mentioning that the φ_{rel}

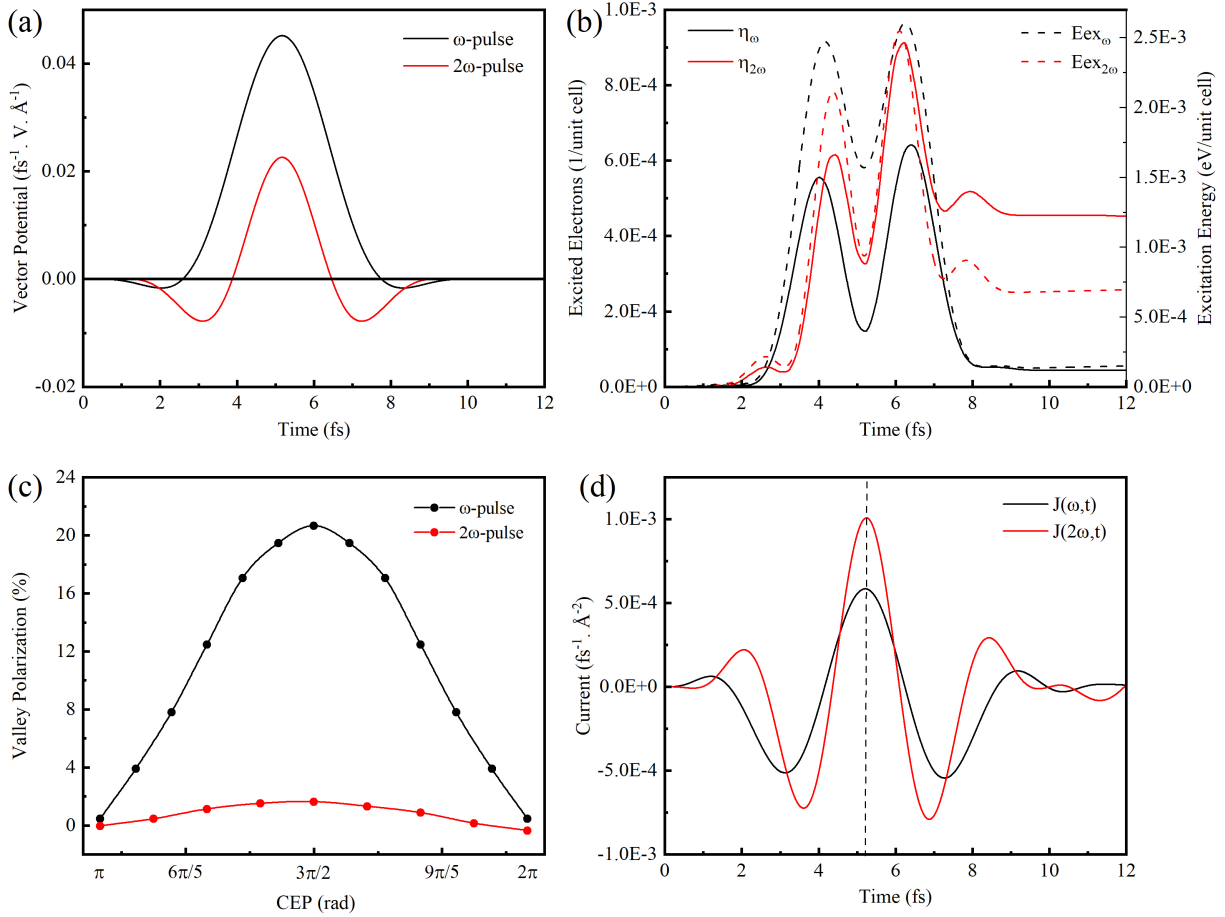


FIG. 1. Comparison of two single-color laser fields with the frequencies of ω and 2ω . Both pulses have the intensity of 10^{10} W/cm 2 . (a) The vector potential (b) The temporal development of excitation energies (E_{ex}) and excited electrons (η) (c) Valley polarization as a function of CEP and (d) The temporal evolution of photocurrents. The CEP in panels (a), (b), and (d) is $3\pi/2$.

dependence changes according to the phase of the fundamental pulse. The valley polarization dependence on φ_{rel} can be explained by the asymmetry of the vector potential and electric field as shown in Fig. 4(b) and (c). Here the asymmetry of the vector potential and the electric field is defined as

$$Asym_{A(E)} = \left| \frac{A_+(E_+)(t)}{A_-(E_-)(t)} \right|, \quad (9)$$

where $A_{\pm}(t)$ and $E_{\pm}(t)$ are the positive (+) and negative (-) peaks of the vector potential and electric field respectively.

Valley polarization and $Asym_{A(t)}$ have strong relevance. i.e smaller vector potential value produces weaker valley polarization while a higher value of $Asym_{A(t)}$ results in a stronger valley polarization. In our calculation, the $Asym_{A(t)}$ (asymmetry of excitation area) dictates the main peak position of valley polarization. However, the peak of the valley polarization may not directly correspond to the maxima of the vector potential. As one can see that the valley polarization peak for $\varphi_{\omega} = 1.625\pi$ is

at 0.625π while the $Asym_{A(t)}$ peak is at 0.375π of $\varphi_{2\omega}$ in Fig. 5. Similarly for $\varphi_{\omega} = 7\pi/4$ the valley peak is at $3\pi/4$ while the $Asym_{A(t)}$ peak is at $\pi/2$ of $\varphi_{2\omega}$. In principle, the peak of valley polarization should follow the $Asym_{A(t)}$ if the tunneling of the electrons is solely responsible for the valley polarization. Even though it is a minor effect, the asymmetric excitation rate due to $E(t)$ influences valley polarization. Since the $Asym_{E(t)}$ is shifted by CEP, the asymmetry of valley polarization shifts slightly by changing CEP.

The peak value of valley polarization in Fig. 4(a) is observed at $\varphi_{2\omega} = \pi/2, 0.625\pi$ and $3\pi/4$. Thus, we have explored the valley polarization at the peaks of $\varphi_{2\omega}$ as a function of φ_{ω} . Fig. 5(a) shows the valley polarization as a function of the φ_{ω} at the peaks of $\varphi_{2\omega}$. The valley polarization curve at various $\varphi_{2\omega}$ nearly overlap. The φ_{ω} dependence of valley polarization shows the same behavior as in the case of a single-color linearly polarized pulse[21, 22], except an increase in the valley polarization value in the second positive half of the sine-like curve. Thus, this valley polarization increase is due to the

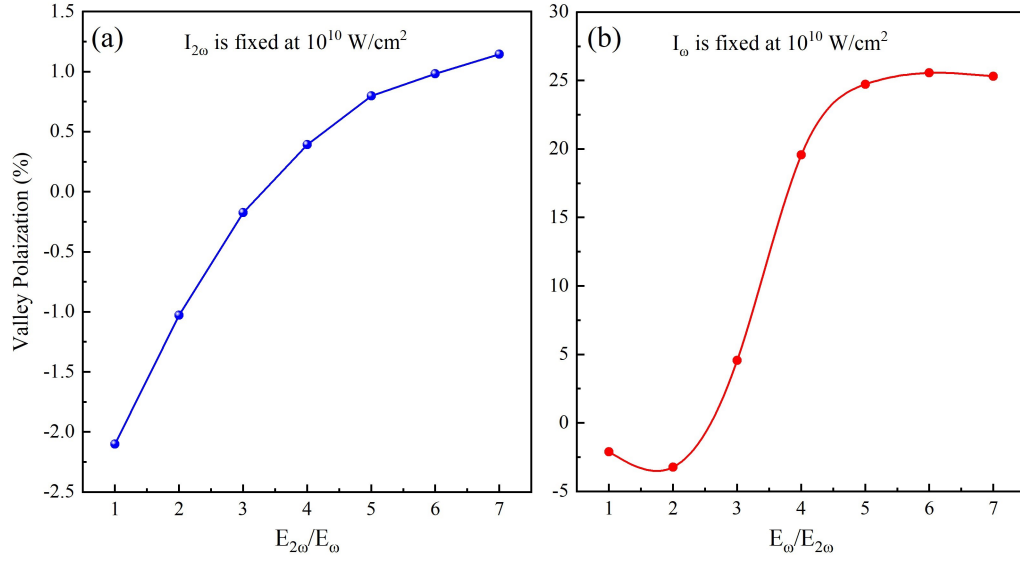


FIG. 2. Valley polarization of the two-color field ($\omega + 2\omega$) field as the function of the ratio between the electric field strengths. (a) The field strength of ω is varied while 2ω is fixed. The CEP is fixed at $\varphi_{\omega} = \pi/2$ and $\varphi_{2\omega} = 3\pi/2$ (b) The field strength of 2ω is varied while ω is fixed. The CEP is fixed at $\varphi_{\omega} = 3\pi/2$ and $\varphi_{2\omega} = \pi/2$. The CEPs are chosen to have a positive peak of valley polarization.

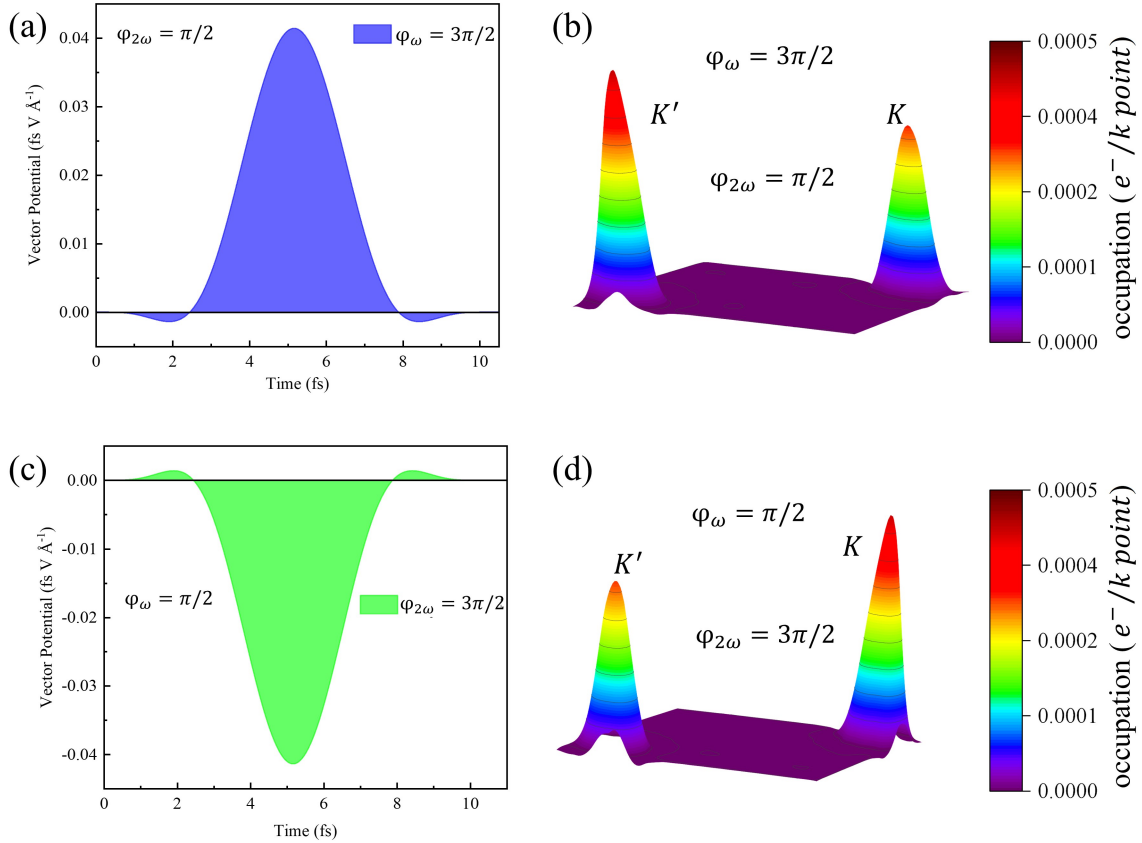


FIG. 3. (a) Vector potential of the $\omega + 2\omega$ field for $\varphi_{\omega} = 3\pi/2$ and $\varphi_{2\omega} = \pi/2$. (b) Conduction band electron populations for the vector potential in (a). The (c) and (d) are the same as (a) and (b) but for $\varphi_{\omega} = \pi/2$, $\varphi_{2\omega} = 3\pi/2$. The electron population is summed over the entire conduction band at the end of the pulse. Two waveforms and their corresponding k -resolved populations are chosen because of their maximum asymmetry and the switching of the valley from K' to K .

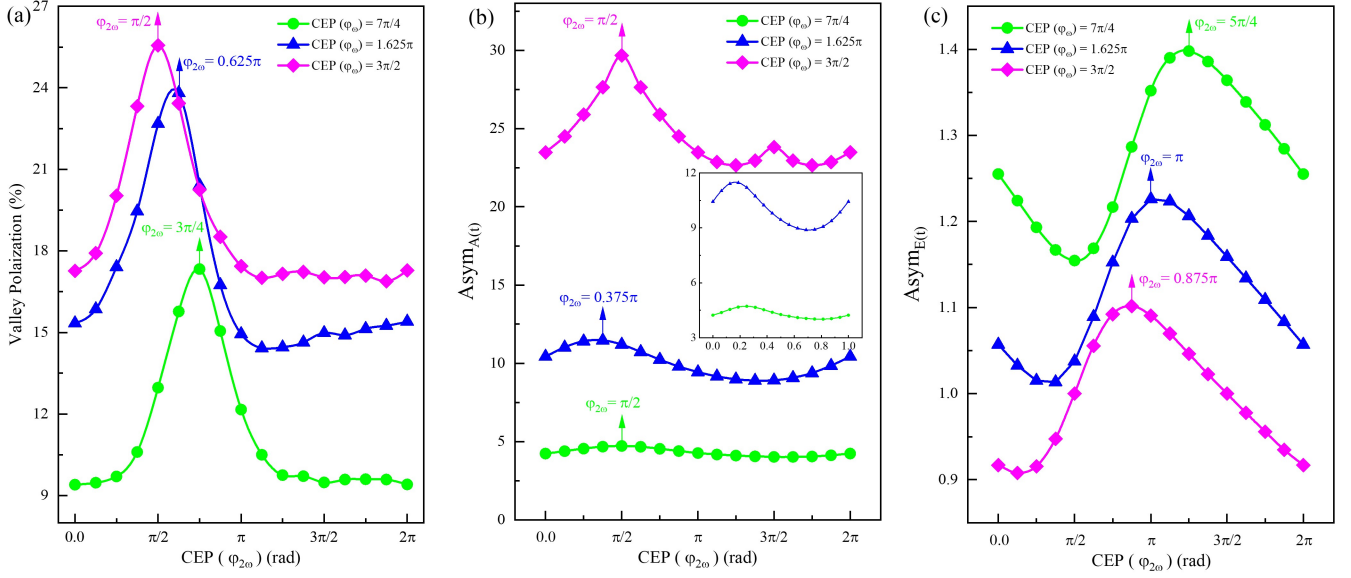


FIG. 4. (a) Valley polarization (b) $Asym_{A(t)}$ and (c) $Asym_{E(t)}$ as a function of $\varphi_{2\omega}$ at specific CEP of ω . The intensity of the $I_{\omega+2\omega} = 0.01 \text{ TWcm}^{-2}$ while the $I_\omega/I_{2\omega} = 36$.

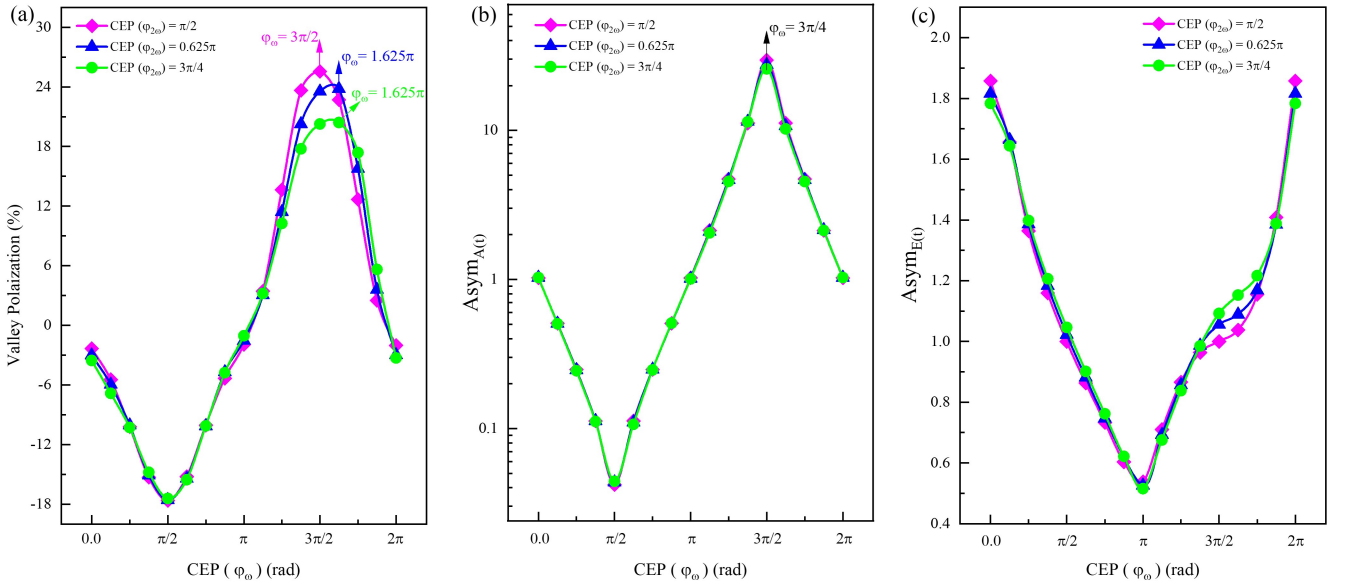


FIG. 5. (a) Valley polarization (b) $Asym_{A(t)}$ and (c) $Asym_{E(t)}$ as a function of φ_ω at maximum valley polarization of $\varphi_{2\omega}$ in Fig. 4(a).

2ω -field. The $Asym_{A(t)}$ in Fig. 5(b) and the $Asym_{E(t)}$ in Fig. 5(c) show very distinctive curves. Due to the predominant tunneling nature of ω -field, the valley polarization nearly follows the $Asym_{A(t)}$ curve as shown in Fig. 5(b). The change in the shoulder structure of $Asym_{E(t)}$ in Fig. 5(c) changes the peak position of valley asymmetry to $\varphi_\omega = 1.625\pi$ for $\varphi_{2\omega} = 0.625\pi$ and $3\pi/4$ which marks the importance of $Asym_{E(t)}$ by $\omega +$

2ω field. Thus the competition between the asymmetry of excitation rate and excitation area by the addition of 2ω -field determines the peak of valley polarization.

IV. CONCLUSION

We have demonstrated the generation of valley polarization in WSe₂ monolayer via $\omega + 2\omega$ superimposed co-linearly laser pulses. The valley polarization induced by $\omega + 2\omega$ pulses is superior to single-color pulse as much as 1.2 times. The intensity ratio and the relative phase between the fundamental pulse and its second harmonic are the most crucial factors in determining valley polarization. Our results indicate that the strong ω mixed with the weaker 2ω enhances the valley polarization. We found that the ratio of $I_\omega/I_{2\omega} = 36$ shows higher valley polarization than the ratio used in molecule cases. The valley polarization is mainly dependent on the CEP of the fundamental pulse. The competition between the asymmetry of the vector potential and electric field mainly determined the maximum valley polarization. Two-color fields provide additional degrees of freedom, such as admixture, polarization, and the relative phase between two pulses. The present scheme helps to understand the ultrafast valley phenomena in 2D layers from the fundamental perspective.

V. AUTHOR INFORMATION

Corresponding Author

*E-mail: otobe.tomohito@qst.go.jp

Author Contributions

Notes

The authors declare no competing financial interest.

VI. ACKNOWLEDGMENT

This research is supported by JST-CREST under Grant No. JP-MJCR16N5. This research is also partially supported by JSPS KAKENHI Grant Nos. 20H02649, 22K13991, and MEXT Quantum Leap Flagship Program (MEXT Q-LEAP) under Grant No. JPMXS0118068681 and JPMXS0118067246. The numerical calculations are carried out using the computer facilities of the Fugaku through the HPCI System Research Project (Project ID: hp220120), SGI8600 at Japan Atomic Energy Agency (JAEA), and Multidisciplinary Cooperative Research Program in CCS, University of Tsukuba.

-
- [1] D. Xiao, G.-B. Liu, W. Feng, X. Xu, and W. Yao, Coupled spin and valley physics in monolayers of mos 2 and other group-vi dichalcogenides, *Physical review letters* **108**, 196802 (2012).
- [2] X. Xu, W. Yao, D. Xiao, and T. F. Heinz, Spin and pseudospins in layered transition metal dichalcogenides, *Nature Physics* **10**, 343 (2014).
- [3] Q. H. Wang, K. Kalantar-Zadeh, A. Kis, J. N. Coleman, and M. S. Strano, Electronics and optoelectronics of two-dimensional transition metal dichalcogenides, *Nature nanotechnology* **7**, 699 (2012).
- [4] J. R. Schaibley, H. Yu, G. Clark, P. Rivera, J. S. Ross, K. L. Seyler, W. Yao, and X. Xu, Valleytronics in 2d materials, *Nature Reviews Materials* **1**, 1 (2016).
- [5] D. Xiao, W. Yao, and Q. Niu, Valley-contrasting physics in graphene: magnetic moment and topological transport, *Physical review letters* **99**, 236809 (2007).
- [6] Y. Shimazaki, M. Yamamoto, I. V. Borzenets, K. Watanabe, T. Taniguchi, and S. Tarucha, Generation and detection of pure valley current by electrically induced berry curvature in bilayer graphene, *Nature Physics* **11**, 1032 (2015).
- [7] E. J. Sie, Valley-selective optical stark effect in monolayer ws 2, in *Coherent Light-Matter Interactions in Monolayer Transition-Metal Dichalcogenides* **346**, 1205 (2014). (Springer, 2018) pp. 37–57.
- [8] T. Cao, G. Wang, W. Han, H. Ye, C. Zhu, J. Shi, Q. Niu, P. Tan, E. Wang, B. Liu, et al., Valley-selective circular dichroism of monolayer molybdenum disulphide, *Nature communications* **3**, 1 (2012).
- [9] A. M. Jones, H. Yu, N. J. Ghimire, S. Wu, G. Aivazian, J. S. Ross, B. Zhao, J. Yan, D. G. Mandrus, D. Xiao, et al., Optical generation of excitonic valley coherence in monolayer wse2, *Nature nanotechnology* **8**, 634 (2013).
- [10] A. K. Geim, Graphene: status and prospects, *science* **324**, 1530 (2009).
- [11] A. C. Neto, F. Guinea, N. M. Peres, K. S. Novoselov, and A. K. Geim, The electronic properties of graphene, *Reviews of modern physics* **81**, 109 (2009).
- [12] Y. Zhang, Y.-W. Tan, H. L. Stormer, and P. Kim, Experimental observation of the quantum hall effect and berry's phase in graphene, *nature* **438**, 201 (2005).
- [13] H. Yuan, X. Wang, B. Lian, H. Zhang, X. Fang, B. Shen, G. Xu, Y. Xu, S.-C. Zhang, H. Y. Hwang, et al., Generation and electric control of spin-valley-coupled circular photogalvanic current in wse2, *Nature nanotechnology* **9**, 851 (2014).
- [14] S. A. Vitale, D. Nezich, J. O. Varghese, P. Kim, N. Gedik, P. Jarillo-Herrero, D. Xiao, and M. Rothschild, Valleytronics: opportunities, challenges, and paths forward, *Small* **14**, 1801483 (2018).
- [15] D. MacNeill, C. Heikes, K. F. Mak, Z. Anderson, A. Kormányos, V. Zólyomi, J. Park, and D. C. Ralph, Breaking of valley degeneracy by magnetic field in monolayer mose 2, *Physical review letters* **114**, 037401 (2015).
- [16] J. Kim, X. Hong, C. Jin, S.-F. Shi, C.-Y. S. Chang, M.-H. Chiu, L.-J. Li, and F. Wang, Ultrafast generation of pseudo-magnetic field for valley excitons in wse2 monolayer, *Physical review letters* **114**, 037401 (2015).
- [17] D. Zhong, K. L. Seyler, X. Linpeng, R. Cheng, N. Sivadas, B. Huang, E. Schmidgall, T. Taniguchi, K. Watanabe, M. A. McGuire, et al., Van der waals engineering of ferromagnetic semiconductor heterostructures for spin and valleytronics, *Science advances* **3**, e1603113 (2017).
- [18] H. Zeng, J. Dai, W. Yao, D. Xiao, and X. Cui, Valley polarization in mos 2 monolayers by optical pumping, *Nature nanotechnology* **7**, 490 (2012).

- [19] K. F. Mak, K. He, J. Shan, and T. F. Heinz, Control of valley polarization in monolayer mos 2 by optical helicity, *Nature nanotechnology* **7**, 494 (2012).
- [20] W. Yao, D. Xiao, and Q. Niu, Valley-dependent optoelectronics from inversion symmetry breaking, *Physical Review B* **77**, 235406 (2008).
- [21] Á. Jiménez-Galán, R. E. Silva, O. Smirnova, and M. Ivanov, Sub-cycle valleytronics: control of valley polarization using few-cycle linearly polarized pulses, *Optica* **8**, 277 (2021).
- [22] A. Hashmi, S. Yamada, A. Yamada, K. Yabana, and T. Otobe, Valley polarization control in wse 2 monolayer by a single-cycle laser pulse, *Physical Review B* **105**, 115403 (2022).
- [23] F. Langer, C. P. Schmid, S. Schlauderer, M. Gmitra, J. Fabian, P. Nagler, C. Schüller, T. Korn, P. Hawkins, J. Steiner, et al., Lightwave valleytronics in a monolayer of tungsten diselenide, *Nature* **557**, 76 (2018).
- [24] P. Kumar, T. M. Herath, and V. Apalkov, Ultrafast valley polarization in bilayer graphene, *Journal of Applied Physics* **130**, 164301 (2021).
- [25] H. K. Kelardeh, U. Saalman, and J. M. Rost, Ultrashort laser-driven dynamics of massless dirac electrons generating valley polarization in graphene, *Physical Review Research* **4**, L022014 (2022).
- [26] J. Theilhaber, Ab initio simulations of sodium using time-dependent density-functional theory, *Physical Review B* **46**, 12990 (1992).
- [27] K. Yabana and G. Bertsch, Time-dependent local-density approximation in real time, *Physical Review B* **54**, 4484 (1996).
- [28] K. Yabana, T. Nakatsukasa, J.-I. Iwata, and G. Bertsch, Real-time, real-space implementation of the linear response time-dependent density-functional theory, *physica status solidi (b)* **243**, 1121 (2006).
- [29] A. D. Laurent and D. Jacquemin, Td-dft benchmarks: a review, *International Journal of Quantum Chemistry* **113**, 2019 (2013).
- [30] A. Castro, M. A. Marques, J. A. Alonso, G. F. Bertsch, and A. Rubio, Excited states dynamics in time-dependent density functional theory, *The European Physical Journal D-Atomic, Molecular, Optical and Plasma Physics* **28**, 211 (2004).
- [31] K. Nobusada and K. Yabana, High-order harmonic generation from silver clusters: Laser-frequency dependence and the screening effect of d electrons, *Physical Review A* **70**, 043411 (2004).
- [32] T. Otobe, M. Yamagiwa, J.-I. Iwata, K. Yabana, T. Nakatsukasa, and G. Bertsch, First-principles electron dynamics simulation for optical breakdown of dielectrics under an intense laser field, *Physical Review B* **77**, 165104 (2008).
- [33] I. Žutić, J. Fabian, and S. D. Sarma, Spintronics: Fundamentals and applications, *Reviews of modern physics* **76**, 323 (2004).
- [34] H. Ohmura, N. Saito, and T. Morishita, Molecular tunneling ionization of the carbonyl sulfide molecule by double-frequency phase-controlled laser fields, *Phys. Rev. A* **89**, 013405 (2014).
- [35] S. Kaziannis, N. Kotsina, and C. Kosmidis, Interaction of toluene with two-color asymmetric laser fields: Controlling the directional emission of molecular hydrogen fragments, *The Journal of Chemical Physics* **141**, 104319 (2014).
- [36] T. Higuchi, C. Heide, K. Ullmann, H. B. Weber, and P. Hommelhoff, Light-field-driven currents in graphene, *Nature* **550**, 224 (2017).
- [37] Á. Jiménez-Galán, R. Silva, O. Smirnova, and M. Ivanov, Lightwave control of topological properties in 2d materials for sub-cycle and non-resonant valley manipulation, *Nature Photonics* **14**, 728 (2020).
- [38] G. F. Bertsch, J.-I. Iwata, A. Rubio, and K. Yabana, Real-space, real-time method for the dielectric function, *Physical Review B* **62**, 7998 (2000).
- [39] S. Yamada, M. Noda, K. Nobusada, and K. Yabana, Time-dependent density functional theory for interaction of ultrashort light pulse with thin materials, *Physical Review B* **98**, 245147 (2018).
- [40] S. Yamada and K. Yabana, Determining the optimum thickness for high harmonic generation from nanoscale thin films: An ab initio computational study, *Physical Review B* **103**, 155426 (2021).
- [41] M. Noda, S. A. Sato, Y. Hirokawa, M. Uemoto, T. Takeuchi, S. Yamada, A. Yamada, Y. Shinohara, M. Yamaguchi, K. Iida, et al., Salmon: Scalable ab-initio light-matter simulator for optics and nanoscience, *Computer Physics Communications* **235**, 356 (2019).
- [42] Salmon official, <http://salmon-tddft.jp>.
- [43] J. P. Perdew and Y. Wang, Accurate and simple analytic representation of the electron-gas correlation energy, *Physical review B* **45**, 13244 (1992).
- [44] U. Von Barth and L. Hedin, A local exchange-correlation potential for the spin polarized case. i, *Journal of Physics C: Solid State Physics* **5**, 1629 (1972).
- [45] T. Oda, A. Pasquarello, and R. Car, Fully unconstrained approach to noncollinear magnetism: application to small fe clusters, *Physical review letters* **80**, 3622 (1998).
- [46] I. Morrison, D. Bylander, and L. Kleinman, Nonlocal hermitian norm-conserving vanderbilt pseudopotential, *Physical Review B* **47**, 6728 (1993).
- [47] H. Liu, Y. Li, Y. S. You, S. Ghimire, T. F. Heinz, and D. A. Reis, High-harmonic generation from an atomically thin semiconductor, *Nature Physics* **13**, 262 (2017).
- [48] N. Yoshikawa, K. Nagai, K. Uchida, Y. Takaguchi, S. Sasaki, Y. Miyata, and K. Tanaka, Interband resonant high-harmonic generation by valley polarized electron-hole pairs, *Nature communications* **10**, 1 (2019).
- [49] H. Ohmura, T. Nakanaga, and M. Tachiya, Coherent control of photofragment separation in the dissociative ionization of ibr, *Phys. Rev. Lett.* **92**, 113002 (2004).